Chemical characteristics of brown carbon in atmospheric particles at a suburban site near Guangzhou, China

Yi Ming Qin[1,#], Hao Bo Tan[2], Yong Jie Li[3], Zhu Jie Li[2,4], Misha I. Schurman[5], Li Liu[2,6], Cheng Wu[7], and Chak K. Chan[1]

[1]School of Energy and Environment, City University of Hong Kong, Hong Kong, China

[2]Key Laboratory of Regional Numerical Weather Prediction, Institute of Tropical and Marine Meteorology, China Meteorological Administration, Guangzhou, China

[3]Department of Civil and Environmental Engineering, Faculty of Science and Technology, University of Macau, Macau, China

[4]School of Environmental Science and Engineering, Nanjing University of Information Science and Technology, Nanjing, China

[5] Zephyr Research Consultants, USA

[6]Department of Atmospheric Science, Sun yat-sen University, Guangzhou, China

[7]Institute of Mass Spectrometer and Atmospheric Environment, Jinan University, Guangzhou, China

[#] now at School of Engineering and Applied Sciences, Harvard University, Cambridge, MA, USA

Correspondence to: Chak K. Chan (chak.k.chan@cityu.edu.hk) and Yong Jie Li (yongjieli@umac.mo)

Abstract:

Light-absorbing organic carbon (or brown carbon, BrC) in atmospheric particles has received much attention for its potential role in global radiative forcing. While a number of field measurement campaigns have differentiated light absorption by black carbon (BC) and BrC, the chemical characteristics of BrC are not well understood. In this study, we present co-located real-time light absorption and chemical composition measurements of atmospheric particles to explore the relationship between the chemical and optical characteristics of BrC at a suburban site downwind of Guangzhou, China from November to December 2014. BrC and BC contributions to light absorption were estimated using measurements from a seven-wavelength aethalometer, while the chemical composition of non-refractory PM_1 was measured with a high resolution time-of-flight aerosol mass spectrometer (HR-ToF-AMS). Using the Absorption Angstrom Exponent (AAE) method, we estimated that BrC contributed 23.6% to the total aerosol absorption at 370 nm, 18.1% at 470 nm, 10.7% at 520 nm, 10.7% at 590 nm, and 10.5% at 660 nm. Biomass burning organic aerosol (BBOA) has the highest mass absorption coefficient among sources of organic aerosols. Its contribution to total brown carbon absorption coefficient decreased but that of low-volatility oxygenated organic aerosol (LVOOA) increased with increasing wavelength, suggesting the need for wavelength-dependent light absorption analysis for BrC in association with its chemical makeup. Clear correlations of N-containing ion fragments with absorption coefficient were observed. These correlations also depended on their degrees of unsaturation/cyclization and oxygenation. While the current study relates light absorption by BrC to ion fragments, more detailed chemical characterization is warranted to constrain this relationship.

Introduction:

Atmospheric particles participate considerably in the global climate direct effect via their light-scattering (e.g., sulfate) and/or light-absorbing components (e.g., black carbon, BC). BC is major contributor to light absorption that leads to positive radiative forcing, increasing the average temperature of the atmosphere. The BrC absorption contribution to total aerosol light absorption can reach 20–50% over regions dominated by seasonal biomass burning and biofuel combustion (Feng et al., 2013).A significant difference in optical feature of BrC and BC is that BrC absorbs light primarily at UV and short-visible wavelengths with the absorption decreasing significantly at long wavelengths, while BC absorbs strongly and constantly throughout the UV to visible spectrum(Andreae and Gelencsér, 2006; Bergstrom et al., 2007; Bond and Bergstrom, 2006). In global climate models, the direct radiative forcing of organic aerosols at the top of atmosphere can shift from cooling (-0.08 Wm^{-2}) to warming ($+0.025$ Wm^{-2}) when strong BrC absorption is included(Feng et al., 2013). However, uncertainties in the sources, formation, chemical composition, and absorption properties of BrC hinder more accurate estimations of radiative forcing induced by atmospheric particles.

BrC is operationally defined and has many chemical constituents, which makes chemical characterization quite challenging. Both primary and secondary organic aerosols can act as BrC (Laskin et al., 2015). For example, biomass burning organic aerosol (BBOA) has been identified as a contributor to BrC in rural areas in the southern United States , while coal combustion organic aerosol (CCOA) contributes substantially to BrC during winter in Beijing (Yan et al., 2017). Species from secondary formation processes, such as humic-like substances (HULIS) formed by in-cloud processing (Rinco et al., 2009), species from gas-phase photo-oxidation of volatile organic compounds (VOCs) in the presence of NO_x, and species from reactions between carbonyl compounds and ammonia in the aqueous film at the particle surface, can also contribute to BrC (Gen et al., 2018; Laskin et al., 2010; Liu et al., 2015). Highly conjugated organics, nitro-aromatic compounds, imidazoles, and other N-heterocyclic compounds have been found in BrC (Laskin et al., 2015; Lin et al., 2016). Sun et al. (2007) also found that light-absorbing organic molecules in BrC are likely large (i.e., possessing > 18 carbon atoms); these molecules are generally highly unsaturated and contain three or more oxygen atoms and/or one or more nitrogen atoms.

The Pearl River Delta (PRD) region, one of the most economically developed regions in China, suffers under air pollution from a variety of sources (Chan and Yao, 2008; Li et al., 2017). Source

apportionment using positive matrix factorization (PMF) analysis of mass spectral data sets from high resolution time-of-flight aerosol mass spectrometry (HR-ToF-AMS) has revealed that the organic aerosol (OA) in this region arises from traffic emissions (i.e., hydrocarbon-like organic aerosol, or HOA), biomass burning (BBOA), cooking (COA), and secondary formation (i.e., oxygenated organic aerosols, or OOAs). In the PRD, HOA is often the largest contributor to OA at urban sites (He et al., 2011), while SOA plays a more important role at rural sites (Gong et al., 2012; Huang et al., 2011). BBOA has also been found to contribute significantly to total OA in the PRD region, with contributions of 24% at an urban site in Shenzhen (He et al., 2011) and 14% and 25% at rural sites in Heshan and Kaiping, respectively (Gong et al., 2012; Huang et al., 2011). Yuan et al. (2016) attributed 6-12% of the total aerosol absorption at 405 nm at a rural site in the PRD to BrC; the authors found higher BrC contributions during fall, which they ascribed to biomass burning (BBOA) activities nearby. However, the BrC components responsible for light absorption remain relatively unknown; this hinders a thorough understanding of the relationships between optical properties and chemical characteristics and, in turn, the realization of a generalized framework that can be extended to other sources and regions.

In this work, we present simultaneous measurements of aerosol chemical composition and light absorption of aerosol particles at a suburban site downwind of Guangzhou in the PRD, China. Contributions of BC and BrC to total aerosol light absorption were differentiated and quantified using measurements from a seven-wavelength aethalometer. Sources of OA, which were determined using PMF analysis, were correlated to BrC light absorption to identify the major contributor(s) to short-wavelength light absorption. More detailed chemical characteristics, such as N-containing ion fragments, the degree of unsaturation (indicated by the ion double bond equivalent, or ion DBE), and the degree of oxygenation (indicated by the number of oxygen atoms in ions), were also used to investigate the structural characteristics of BrC related to light absorption.

Methodology

1. Sampling site

We conducted field measurements at the Guangzhou Panyu Atmospheric Composition Station (GPACS, 23°00′ N, 113°21′ E), on the periphery of Guangzhou, China, from November 7, 2014

to January 3, 2015. The GPACS is located on top of a hill with an altitude of approximately 150 m a.s.l. (Cheung et al., 2016; Tan et al., 2013; Zou et al., 2015); it is approximately 15 km south of the city center and was downwind of the central city throughout the sampling period, during which north winds prevailed (Qin et al., 2017).

2. Measurements and data analysis

Aerosol light absorption was measured with a seven-wavelength aethalometer (Magee Scientific, model AE33) at 370, 470, 520, 590, 660, 880, and 950 nm. Ambient air was drawn through a 2.5-μm cut-off inlet at 2 L/min before entering the aethalometer; particles were collected on the filter substrate, and light attenuation at the wavelengths above was recorded continuously. A diffusion drier was used to dry the sampled air stream, which reduced the RH of the air to below 30 %. The optical properties of the collected particles were determined by comparing light attenuation in particle-laden and particle-free filter areas (Weingartner et al., 2003). To convert aerosol particles light attenuation coefficients at the filter substrate to the light absorption coefficients suspended in the air, a real-time compensation parameter k and a fixed multiple scattering parameter C were used. The real-time loading effect correction was performed using two parallel measurements of optical attenuations at different accumulation rates. C_{ref} =2.14 for quartz filter and C_{ref}=1.57 for tetrafluoroethylene (TFE)-coated glass filter were recommended from previously studies for the fresh soot particles (Drinovec et al., 2015; Weingartner et al., 2003). However, with the presence of semi-volatile oxidation products, significantly higher values (C =3.6±0.6) were observed in the organic coating experiment using a quartz filter (Weingartner et al., 2003). Wavelength dependence of C has also been reported in the literature (Arnott et al., 2005; Schmid et al., 2006; Segura et al., 2014) . A broad range of C (from 2.8 to 7.8) at several sites was also used by Collaud Coen et al. (2010). As the multiple scattering parameter (C) may be site specific, we further compared the absorption from AE33 with cavity ring-down spectroscopy (CRD, Hexin XG-1000) and Nephelometer (TSI, 3563). The nephelometer was calibrated by CO_2 weekly during the field campaign. Particle-free air was checked once a day. The CRD was calibrated using polystyrene spheres with known indices of refraction before the campaign. We extracted the light absorption based on extinction and scattering measurements from cavity ring-down spectroscopy and Nephelometer, respectively, as below.

$$b_{abs} = \sigma_{ext} - \sigma_{sp} \quad (1)$$

where b_{abs}, σ_{ext} and σ_{sp} are absorption coefficient, extinction coefficient and scattering coefficient.

The scatter plot of absorption at 532 nm from measurement from the aethalometer (AE33) and that calculated from CRD and Nephelometer (CRD-Neph) is displayed in Figure 1. AE 33 absorption coefficient was higher than the absorption estimated from Eq. 1. by a factor of 2.10. Therefore, the final multiple scattering parameter (C) was set to $C_{final} = C_{ref} \times 2.10 = 3.29$. This value is comparable with previous aethalometer measurements (C=3.48) in the PRD region (Wu et al., 2009, 2013).

The non-refractory chemical composition of submicron aerosols was measured with an Aerodyne HR-ToF-AMS (Aerodyne Research Inc., Billerica, MA, USA). Briefly, the AMS collected five-minute-average particle mass spectra for the high-sensitivity V plus particle time-of-flight (PToF) mode and the high-resolution W mode. AMS data analysis was performed using the SQUIRREL (v1.56D) and PIKA (v1.15D) toolkits in Igor Pro (WaveMetrics Inc., Lake Oswego, OR). Source apportionment was performed via PMF analysis with Multilinear Engine 2 (ME-2) via the SoFi interface (Canonaco et al., 2013). Five factors, including HOA, COA, BBOA, semi-volatile oxygenated organic aerosol (SVOOA), and low-volatility oxygenated organic aerosol (LVOOA), were resolved (Qin et al., 2017). The campaign average OA composition was dominated by surrogates of SOA (SVOOA + LVOOA). However, freshly-emitted hydrocarbon-like organic aerosols (HOA) contributed up to 40.0% of OA during high-OA periods; during nighttime, HOA contributed 23.8% to 28.4% on average. BBOA contributed 9.6% (1.87 μg/m^3) of total OA in November and 6.5% (1.38 μg/m^3) in December. AMS data treatment was discussed in detail in Qin et al. (2017). Data from a thermo-optical elemental carbon and organic carbon (ECOC) analyzer (Sunset Laboratory Inc.) were also used for comparison.

Results and discussion

1. Aerosol absorption

Figure 2a shows the box-whisker plot of aerosol absorption coefficients (b_{abs}) from 370 nm to 950 nm from the aethalometer measurements during the campaign. The campaign-average absorption coefficients were 56.00 Mm^{-1} at 370 nm, 40.99 Mm^{-1} at 470 nm, 34.76 Mm^{-1} at 520 nm, 29.91 Mm^{-1} at 590 nm, 26.69 Mm^{-1} at 660 nm, 18.06 Mm^{-1} at 880 nm, and 16.71 Mm^{-1} at 950 nm.

In multi-wavelength absorption measurements, the total absorption Ångström exponent (AAE) can be calculated by a power-law fitting of the absorption coefficient over all available wavelengths. AAE of unity has been widely used for pure black carbon, while a shift to higher AAE value has been observed with the presence of brown carbon. The reason behind is that BrC has a much stronger absorption at UV and short visible wavelengths than at long visible wavelengths, which yields a steeper curve (Andreae and Gelencsér, 2006; Bergstrom et al., 2007; Bond and Bergstrom, 2006). The presence of non-absorbing OA shells over BC cores may also lead to a shift of AAE (Gyawali et al., 2009). This latter possibility is analyzed in a separated manuscript (Li et al., in preparation). Briefly, a Mie theory model was used to estimate the AAE for BC-containing particles (AAE_{BC}) at core-shell scenarios with different refractive indexes. AAE_{BC} is sensitive to specific refractive index of core and shell of the particles and the size of the particle. The size distribution is from scanning mobility particle sizer and aerodynamic particle sizer measurement, and we vary the refractive index of the core and shell in the model. The method is adopted from Tan et al. (2016) . In general, AAEBC increases as the real part refractive index of the core increases or the imaginary decreases, or alternatively real part of the shell increases. The AAE_{BC} ranges from 0.67-1.03 across the different scenario (Table S1). As shown in Figure 2b, the AAE values, which average at 1.43, are almost always higher than 1, indicating appreciable contributions from BrC to particle light absorption at this site.

To further explore the importance of BrC at this site, BrC absorption at a short wavelength λ_1 ($b_{BrC,\lambda 1}$) can be derived by subtracting BC absorption ($b_{BC,\lambda 1}$) from the total aerosol absorption (Lack and Langridge, 2013) via:

$$b_{BrC,\lambda 1} = b_{\lambda 1} - b_{BC,\lambda 1} \quad (2)$$

where absorption $b_{\lambda 1}$ is the measured absorption at the short wavelength λ_1. BC absorption at λ_1 ($b_{BC,\lambda 1}$) can be obtained from the AAE value of BC (AAE_{BC}) via:

$$b_{BC,\lambda 1} = b_{\lambda 2} \times (\lambda_2 / \lambda_1)^{AAE_{BC}} \quad (3)$$

where $b_{\lambda 2}$ is the absorption at a longer wavelength λ_2 (880 nm), which is assumed to have no contributions from BrC or dust (Drinovec et al., 2015; Zhu et al., 2017). The uncertainty involved in attributing BrC and BC absorption at short wavelengths has been explored explicitly by Lack

and Langridge (2013). This uncertainty is primarily from uncertainty of choice of AAE_{BC}. Based on the AAE_{BC} from Mie theory model, a sensitivity analysis of BrC contribution to total light absorption is presented in Figure S1.

Figure 3 shows the b_{abs} attributed to BC and BrC (b_{BC} and b_{BrC}) at different wavelengths. Aerosol light absorption coefficients were dominated by BC, but b_{BrC} was not negligible, especially at short wavelengths. The campaign-average b_{BrC} values were 13.67, 7.56, 4.49, 3.22, and 2.81 Mm^{-1} at 370, 470, 520, 590, and 660 nm, respectively; BrC absorption contributed 23.6%, 18.1%, 10.7%, 10.7%, and 10.5% of the total absorption at the corresponding wavelengths. The proportions of BrC and BC in our campaign were slightly higher than those reported an earlier study in the PRD by Yuan et al. (2016). In their study, the average light absorption contributions of BrC during Shenzhen winter, Shenzhen fall, and Heshan fall campaigns were 11.7%, 6.3%, and 12.1% at 405 nm and 10.0%, 4.1%, and 5.5% at 532 nm, respectively.

Figure 4 shows the diurnal variations of both b_{BrC} and b_{BC} at 370, 470, 520, 590, and 660 nm, respectively. In general, the diurnal cycles of b_{BrC} and b_{BC} share similar patterns, indicating that they may have similar sources. However, it should be noted that some OA factors, such as BBOA and HOA, also share similar patterns(Qin et al., 2017). Overall, there were two peaks at each wavelength. The first peak appeared in the morning at around 8:00 LT, with a peak before 8:00 LT for longer wavelength and after 8:00 LT for shorter wavelength. The second peak appeared at 21:00 LT and its intensity decreased until 24:00 LT. These changes may be attributed to diurnal changes in BrC sources, which most likely originated from crop residual burning in fall and winter in nearby regions (Wang et al., 2017). The diurnal variations of the different wavelengths were not significantly different, although short wavelengths exhibited more obvious diurnal variations.

2. Correlation of light absorption by BrC with OA components

To explore the possible sources of BrC, correlations were determined between b_{BrC} at 370 nm ($b_{BrC,370}$) and various OA types. Data at 370 nm were chosen (over data at longer wavelengths) for their higher signal-to-noise ratios and larger contributions of BrC to light absorption. Figure 5 shows that BBOA concentrations and $b_{BrC,370}$ were well correlated (Pearson's correlation coefficient, R_p = 0.58). More interestingly, a moderate correlation (Rp = 0.40) was also found between $b_{BrC,370}$ and the LVOOA mass concentration. Although the LVOOA factor was not further resolved into OOA factors with biomass origins, it is likely that a portion of LVOOA was formed

from biomass burning precursors through either gas-phase oxidation or heterogeneous reactions. Satish et al. (2017) found correlations between BrC absorption and both primary BBOA and BBOA-related SVOOA factors. They also reported that the slope of the correlation between $b_{BrC,370}$ and BBOA (slope = 1.35) was 4.8 times higher than that between $b_{brc,370}$ and one of the biomass burning SVOOA factors (slope = 0.28), indicating that aging may have reduced the absorption capacity of biomass-related OA.

Multiple regression analysis was also used to resolve the correlation factors of each OA component ($m^2\ g^{-1}$) at each wavelength.

$$b_{BrC} = a*[HOA]+b*[COA]+c*[BBOA]+d*[SVOOA]+e*[LVOOA] \quad (4)$$

where a, b, c, d, e indicates the correlation factors of each OA component ($m^2\ g^{-1}$) and [..] indicates the mass concentration of each OA component. These correlation factors obtained are equivalent to MAC mass absorption coefficient (MAC) of each OA component. We will use these factors to compare with MAC reported in the literature later.

Washenfelder et al. (2015) reported a MAC of 1.3 ± 0.06 $m^2\ g^{-1}$ using the b_{BrC} at 365 nm for BBOA in the rural southeastern United States, which was 40 to 135 times higher than the MAC values reported for other OA factors. Di Lorenzo et al. (2017) found that both BBOA and more-oxidized oxygenated organic aerosol (MO-OOA) were associated with water soluble BrC and that the MAC of BBOA doubled that of MO-OOA. However, Forrister et al. (2015) observed that BrC in wildfire plumes had a lifetime of roughly 9 to 15 hours, probably due to conversion to SOA with lower light absorption capacity. In our study, the MAC (correlation factor in Table 1) of BBOA at 370 nm was 3.4 ± 0.41 $m^2\ g^{-1}$, roughly 3.4 times that of LVOOA (1.04 ± 0.08 $m^2\ g^{-1}$). Like the studies listed above (Forrister et al., 2015; Di Lorenzo et al., 2017; Washenfelder et al., 2015), our results suggest that the absorption coefficient of nascent BBOA is higher than that of its aged counterpart at short wavelength. However, it should be noted that LVOOA might consist of some other non-absorbing SOA components with no biomass origin. It is therefore important to consider chromophore lifetimes when modeling light absorption by BrC. As noted in Laskin et al. (2015), the physicochemical properties of chromophores in BrC may exhibit dynamic changes that are not yet sufficiently understood. In addition, the difference between MAC values of BBOA and LVOOA decreased for longer wavelengths. The MAC values of BBOA were roughly 3.4, 1.8, 1.5, 1.48, and 0.80 times those of LVOOA at 370, 470, 520, 570, and 660 nm, respectively. The

contribution to total absorption coefficient also varied with wavelengths. The contribution from BBOA decrease from 25.8% to 10.1% from 370 nm to 660 nm, while the contribution from LVOOA increase from 49.3% to 60.2 % from 370nm to 660nm. The contribution of HOA was more stable across different wavelengths but was also significant, likely due to the high mass concentration of HOA. The exponential decay of b_{abs} for different light-absorbing components was shown in Figure 7. The fitted AAE values for those components are 3.52, 3.28, 5.50 and 2.67 for total BrC, HOA, BBOA and LVOOA respectively. These results indicate that variability of AAE values ranging from different sources which is likely inherent to the chemical variability of BrC constituents. Altogether, these observations indicate that the wavelength-dependent light absorption of different OAs must be considered in light absorption models.

3. Correlation of b_{BrC} with N-containing organic ions

The chromophores in BrC that are responsible for OA light absorption are not well characterized. Structurally, light absorption depends on the extent of sp^2 hybridization, in which π electrons are usually found (Bond and Bergstrom, 2006). Of the elements commonly found in OA, both C and N have strong tendencies toward sp^2 hybridization. It has also been found that, despite their small OA mass fraction contributions, N-containing organic species in OA can be responsible for appreciable light absorption (Chen et al., 2016; Laskin et al., 2015). Thus, we examined the correlations between b_{BrC} and N-containing ions from AMS measurements. These ion fragments, including the $C_xH_yN^+$ and $C_xH_yO_zN^+$families, likely originated from N-heterocyclic compounds. Figure 6 shows that the mass loadings of $C_xH_yN^+$ and $C_xH_yO_zN^{++}$ families are correlated with b_{BrC} at 370 nm and that correlations are stronger for fragments containing both N and O atoms. These results are consistent with Chen et al. (2016), who suggested that organic compounds with O and N atoms might contribute substantially to total light absorption and fluorescence in OA components.

The effects of oxygenation (as indicated by the number of O atoms in an ion) and unsaturation/cyclization (as indicated by the ion double bond equivalent, or ion DBE) were also examined for each $C_xH_yN^+$ and $C_xH_yO_zN^+$ ion family. Several studies found that species with high DBE values may have substantial network of conjugated double bonds and likely contribute to light absorption (Budisulistiorini et al., 2017; Laskin et al., 2014; Lin et al., 2016). The ion DBE

represents the number of double bonds (unsaturation) or rings (cyclization) that an ion contains and is calculated on the basis of the elemental formula via the following equation:

$$DBE = C + 1 - H/2 - X/2 + N/2 \quad (4)$$

where C, H, X, and N are the number of carbon, hydrogen, halogen (Cl, Br, I, and F), and nitrogen atoms present in the ion, respectively.

Figure 8a shows the correlation coefficients between bBrC at all available wavelengths and the mass loadings of each ion in $C_xH_yN^+$ and $C_xH_yNO_z^+$ families at different DBE values. For the $C_xH_yN^+$family, R_p increased as DBE increased across all wavelength, suggesting that bBrC was better correlated with fragments with higher degrees of unsaturation or cyclization. And increasing trend of Rp as DBE increased is more obvious for short wavelengths (e.g. λ at 370 nm and 470 nm), suggesting that the absorption at short wavelengths are more associated with the unsaturation or cyclization. Indeed, in saturated organics, light absorption involves excitation of n electrons, which requires more energy and, therefore, shorter incident wavelengths (e.g., short UV). In unsaturated organics, the delocalized π electrons are in clusters of sp2 hybrid bonds and in longer conjugated systems, such that the energy difference between the excited state and the ground state goes down, which makes the absorption band shift to longer wavelengths. These structural features may explain in part the increased correlation between mass loadings of the $C_xH_yN^+$ family and light absorption with decreasing ion saturation. For the $C_xH_yNO_z^+$ family, we did not observe obvious trends in the correlation coefficient with changing degree of saturation/cyclization (Figure 8b). This phenomenon is consistent across different wavelength. However, the overall Pearson's Rs of b_{BrC} with $C_xH_yNO_z^+$ were higher than those with $C_xH_yN^+$. The Rp for each group of ions is higher at short wavelengths (λ at 370 nm and 470 nm).

Conclusions

This paper presents collocated, real-time atmospheric particle light absorption and chemical composition measurements at a suburban site in PRD, China. While BC dominated aerosol light absorption, BrC also contributed to absorption at short wavelengths. The aerosol light absorption coefficients of BrC were 13.67, 7.56, 4.49, 3.22, and 2.81 Mm^{-1} at 370, 470, 520, 590, and 660 nm, respectively, and BrC contributed 23.6%, 18.1%, 10.7%, 10.7%, and 10.5% of the total absorption at the corresponding wavelengths. Hydrocarbon-like organic aerosol (HOA), biomass burning

organic aerosol (BBOA) and low-volatility oxygenated organic aerosol (LVOOA) were also substantial for the source of BrC. At short wavelength (370 nm), the mass absorption coefficient of BBOA was higher than those of HOA and LVOOA. However, the difference between the mass absorption coefficients of BBOA and other OA factors decreased with increasing wavelength. The contribution of different OA sources to total absorption coefficient also varied with wavelengths. Such a wavelength dependent trend is also observed for their contribution to total BrC absorption coefficients. $C_xH_yN^+$ and $C_xH_yO_zN^+$, were likely the chromophores responsible for the observed BrC light absorption. The mass loadings of $C_xH_yN^+$ and $C_xH_yO_zN^+$ ion families became better correlated with the BrC light absorption coefficient as their degrees of unsaturation/cyclization and oxygenation increased. This study shows wavelength-dependent light absorption by BrC is strongly influenced by moderately specific molecular characteristics such as degrees of unsaturation/ cyclization and oxygenation. An exploration of the absorptive properties of more specific molecular features, such as the chemical identities of BrC constituents, would require a more detailed chemical characterization of the highly complex OA composition.

Acknowledgements

This work was supported by the National Key Project of the Ministry of Science and Technology of the People's Republic of China (2016YFC0201901, 2016YFC0203305). The authors would like to acknowledge Hong Kong University of Science and Technology for the use of their AMS. We also thank Jianhuai Ye for fruitful discussion. Chak K. Chan would like to acknowledge the Science Technology and Innovation Committee of Shenzhen municipality (project no. 41675117). Yong Jie Li gratefully acknowledges support from Science and Technology Development Fund of Macau (FDCT-136/2016/A3).

References

Andreae, M. O. and Gelencsér, A.: Black carbon or brown carbon? The nature of light-absorbing carbonaceous aerosols, Atmos. Chem. Phys., 6(3), 3419–3463, doi:10.5194/acpd-6-3419-2006, 2006.

Arnott, W. P., Hamasha, K., Moosmüller, H., Sheridan, P. J. and Ogren, J. A.: Towards aerosol light-absorption measurements with a 7-wavelength aethalometer: Evaluation with a photoacoustic instrument and 3-wavelength nephelometer, Aerosol Sci. Technol., 39(1), 17–29, doi:10.1080/027868290901972, 2005.

Bergstrom, R. W., Pilewskie, P., Russell, P. B., Redemann, J., Bond, T. C., Quinn, P. K. and Sierau, B.: Spectral absorption properties of atmospheric aerosols, Atmos. Chem. Phys., 7(23), 5937–5943, doi:10.5194/acp-7-5937-2007, 2007.

Bond, T. C. and Bergstrom, R. W.: Light Absorption by Carbonaceous Particles: An Investigative Review, Aerosol Sci. Technol., 40(1), 27–67, doi:10.1080/02786820500421521, 2006.

Budisulistiorini, S. H., Riva, M., Williams, M., Chen, J., Itoh, M., Surratt, J. D. and Kuwata, M.: Light-Absorbing Brown Carbon Aerosol Constituents from Combustion of Indonesian Peat and Biomass, Environ. Sci. Technol., 51(8), 4415–4423, doi:10.1021/acs.est.7b00397, 2017.

Canonaco, F., Crippa, M., Slowik, J. G., Baltensperger, U. and Prévôt, A. S. H.: SoFi, an IGOR-based interface for the efficient use of the generalized multilinear engine (ME-2) for the source apportionment: ME-2 application to aerosol mass spectrometer data, Atmos. Meas. Tech., 6(12), 3649–3661, doi:10.5194/amt-6-3649-2013, 2013.

Chan, C. K. and Yao, X.: Air pollution in mega cities in China, Atmos. Environ., 42(1), 1–42, doi:10.1016/j.atmosenv.2007.09.003, 2008.

Chen, Q., Ikemori, F. and Mochida, M.: Light Absorption and Excitation-Emission Fluorescence of Urban Organic Aerosol Components and Their Relationship to Chemical Structure, Environ. Sci. Technol., 50(20), 10859–10868, doi:10.1021/acs.est.6b02541, 2016.

Cheung, H. H. Y., Tan, H., Xu, H., Li, F., Wu, C., Yu, J. Z. and Chan, C. K.: Measurements of non-volatile aerosols with a VTDMA and their correlations with carbonaceous aerosols in Guangzhou, China, Atmos. Chem. Phys., 16(13), 8431–8446, doi:10.5194/acp-16-8431-2016, 2016.

Collaud Coen, M., Weingartner, E., Apituley, A., Ceburnis, D., Fierz-Schmidhauser, R., Flentje, H., Henzing, J. S., Jennings, S. G., Moerman, M., Petzold, A., Schmid, O. and Baltensperger, U.: Minimizing light absorption measurement artifacts of the Aethalometer: Evaluation of five correction algorithms, Atmos. Meas. Tech., 3(2), 457–474, doi:10.5194/amt-3-457-2010, 2010.

Drinovec, L., Močnik, G., Zotter, P., Prévôt, A. S. H., Ruckstuhl, C., Coz, E., Rupakheti, M., Sciare, J., Müller, T., Wiedensohler, A. and Hansen, A. D. A.: The "dual-spot" Aethalometer: An improved measurement of aerosol black carbon with real-time loading compensation, Atmos. Meas. Tech., 8(5), 1965–1979, doi:10.5194/amt-8-1965-2015, 2015.

Feng, Y., Ramanathan, V. and Kotamarthi, V. R.: Brown carbon: A significant atmospheric

absorber of solar radiation, Atmos. Chem. Phys., 13(17), 8607–8621, doi:10.5194/acp-13-8607-2013, 2013.

Forrister, H., Liu, J., Scheuer, E., Dibb, J., Ziemba, L., Thornhill, K. L., Anderson, B., Diskin, G., Perring, A. E., Schwarz, J. P., Campuzano-Jost, P., Day, D. A., Palm, B. B., Jimenez, J. L., Nenes, A. and Weber, R. J.: Evolution of brown carbon in wildfire plumes, Geophys. Res. Lett., 42(11), 4623–4630, doi:10.1002/2015GL063897, 2015.

Gen, M., Huang, D. and Chan, C. K.: Reactive uptake of glyoxal by ammonium containing salt particles as a function of relative humidity, Environ. Sci. Technol., 52, 6903–6911, doi:10.1021/acs.est.8b00606, 2018.

Gong, Z., Lan, Z., Xue, L., Zeng, L., He, L. and Huang, X.: Characterization of submicron aerosols in the urban outflow of the central Pearl River Delta region of China, Front. Environ. Sci. Eng. China, 6(5), 725–733, doi:10.1007/s11783-012-0441-8, 2012.

Gyawali, M., Arnott, W. P., Lewis, K. and Moosmüller, H.: In situ aerosol optics in Reno, NV, USA during and after the summer 2008 California wildfires and the influence of aerosol coatings, Atmos. Chem. Phys. Discuss., 9, 8007–8015, doi:10.5194/acp-9-8007-2009, 2009.

He, L.-Y., Huang, X.-F., Xue, L., Hu, M., Lin, Y., Zheng, J., Zhang, R. and Zhang, Y.-H.: Submicron aerosol analysis and organic source apportionment in an urban atmosphere in Pearl River Delta of China using high-resolution aerosol mass spectrometry, J. Geophys. Res., 116(D12), D12304, doi:10.1029/2010JD014566, 2011.

Huang, X.-F. F., He, L.-Y. Y., Hu, M., Canagaratna, M. R., Kroll, J. H., Ng, N. L., Zhang, Y.-H. H., Lin, Y., Xue, L., Sun, T.-L. L., Liu, X.-G. G., Shao, M., Jayne, J. T. and Worsnop, D. R.: Characterization of submicron aerosols at a rural site in Pearl River Delta of China using an Aerodyne High-Resolution Aerosol Mass Spectrometer, Atmos. Chem. Phys., 11(5), 1865–1877, doi:10.5194/acp-11-1865-2011, 2011.

Lack, D. A. and Langridge, J. M.: On the attribution of black and brown carbon light absorption using the angstrom exponent, Atmos. Chem. Phys., 13(20), 10535–10543, doi:10.5194/acp-13-10535-2013, 2013.

Laskin, A., Laskin, J. and Nizkorodov, S. a.: Chemistry of Atmospheric Brown Carbon, Chem. Rev., 115(10), 4335–4382, doi:10.1021/cr5006167, 2015.

Laskin, J., Laskin, A., Roach, P. J., Slysz, G. W., Anderson, G. A., Nizkorodov, S. A., Bones, D. L. and Nguyen, L. Q.: Mass Spectrometry for Chemical Characterization of Organic Aerosols, , 82(5), 2048–2058, doi:10.1029/2007JD008683, 2010.

Laskin, J., Laskin, A., Nizkorodov, S. A., Roach, P., Eckert, P., Gilles, M. K., Wang, B., Lee, H. J. and Hu, Q.: Molecular selectivity of brown carbon chromophores, Environ. Sci. Technol., 48(20), 12047–12055, doi:10.1021/es503432r, 2014.

Li, Y. J., Sun, Y., Zhang, Q., Li, X., Li, M., Zhou, Z. and Chan, C. K.: Real-time chemical characterization of atmospheric particulate matter in China : A review, Atmos. Environ., 158, 270–304, doi:10.1016/j.atmosenv.2017.02.027, 2017.

Lin, P., Aiona, P. K., Li, Y., Shiraiwa, M., Laskin, J., Nizkorodov, S. A. and Laskin, A.: Molecular Characterization of Brown Carbon in Biomass Burning Aerosol Particles, Environ.

Sci. Technol., 50(21), 11815–11824, doi:10.1021/acs.est.6b03024, 2016.

Liu, P. F., Abdelmalki, N., Hung, H. M., Wang, Y., Brune, W. H. and Martin, S. T.: Ultraviolet and visible complex refractive indices of secondary organic material produced by photooxidation of the aromatic compounds toluene and m-xylene, Atmos. Chem. Phys., 15(3), 1435–1446, doi:10.5194/acp-15-1435-2015, 2015.

Di Lorenzo, R. A., Washenfelder, R. A., Attwood, A. R., Guo, H., Xu, L., Ng, N. L., Weber, R. J., Baumann, K., Edgerton, E. and Young, C. J.: Molecular-Size-Separated Brown Carbon Absorption for Biomass-Burning Aerosol at Multiple Field Sites, Environ. Sci. Technol., 51(6), 3128–3137, doi:10.1021/acs.est.6b06160, 2017.

Massabo, D., Caponi, L., Bernardoni, V., Bove, M. C., Brotto, P., Calzolai, G., Cassola, F., Chiari, M., Fedi, M. E., Fermo, P., Giannoni, M., Lucarelli, F., Nava, S., Piazzalunga, A., Valli, G., Vecchi, R. and Prati, P.: Multi-wavelength optical determination of black and brown carbon in atmospheric aerosols, Atmos. Environ., 108, 1–12, doi:10.1016/j.atmosenv.2015.02.058, 2015.

Qin, Y. M., Tan, H. B., Li, Y. J., Schurman, M. I., Li, F., Canonaco, F., Prévôt, A. S. H. and Chan, C. K.: Impacts of traffic emissions on atmospheric particulate nitrate and organics at a downwind site on the periphery of Guangzhou, China, Atmos. Chem. Phys., 2017(x), 1–31, doi:10.5194/acp-2017-116, 2017.

Rinco, A. G., Guzma, M. I., Hoffmann, M. R. and Colussi, A. J.: Optical Absorptivity versus Molecular Composition of Model Organic Aerosol Matter, , 10512–10520, 2009.

Satish, R., Shamjad, P., Thamban, N., Tripathi, S. and Rastogi, N.: Temporal Characteristics of Brown Carbon over the Central Indo- Gangetic Plain, , doi:10.1021/acs.est.7b00734, 2017.

Schmid, O., Artaxo, P., Arnott, W. P., Chand, D., Gatti, L. V., Frank, G. P., Hoffer, A., Schnaiter, M. and Andreae, M. O.: Spectral light absorption by ambient aerosols influenced by biomass burning in the Amazon Basin. I: Comparison and field calibration of absorption measurement techniques, Atmos. Chem. Phys., 6(11), 3443–3462, doi:10.5194/acp-6-3443-2006, 2006.

Segura, S., Estellés, V., Titos, G., Lyamani, H., Utrillas, M. P., Zotter, P., Prévôt, A. S. H., Močnik, G., Alados-Arboledas, L. and Martínez-Lozano, J. A.: Determination and analysis of in situ spectral aerosol optical properties by a multi-instrumental approach, Atmos. Meas. Tech., 7(8), 2373–2387, doi:10.5194/amt-7-2373-2014, 2014.

Sun, H., Biedermann, L. and Bond, T. C.: Color of brown carbon : A model for ultraviolet and visible light absorption by organic carbon aerosol, , 34(August), 1–5, doi:10.1029/2007GL029797, 2007.

Tan, H., Yin, Y., Gu, X., Li, F., Chan, P. W., Xu, H., Deng, X. and Wan, Q.: An observational study of the hygroscopic properties of aerosols over the Pearl River Delta region, Atmos. Environ., 77, 817–826, doi:10.1016/j.atmosenv.2013.05.049, 2013.

Tan, H., Liu, L., Fan, S., Li, F., Yin, Y., Cai, M. and Chan, P. W.: Aerosol optical properties and mixing state of black carbon in the Pearl River Delta, China, Atmos. Environ., 131, 196–208, doi:10.1016/j.atmosenv.2016.02.003, 2016.

Wang, Y., Hu, M., Lin, P., Guo, Q., Wu, Z., Li, M., Zeng, L., Song, Y., Zeng, L., Wu, Y., Guo, S., Huang, X. and He, L.: Molecular Characterization of Nitrogen-Containing Organic Compounds in Humic-like Substances Emitted from Straw Residue Burning, Environ. Sci. Technol., 51(11), 5951–5961, doi:10.1021/acs.est.7b00248, 2017.

Washenfelder, R. A., Attwood, A. R., Brock, C. A., Guo, H., Xu, L., Weber, R. J., Ng, N. L., Allen, H. M., Ayres, B. R., Baumann, K., Cohen, R. C., Draper, D. C., Duffey, K. C., Edgerton, E., Fry, J. L., Hu, W. W., Jimenez, J. L., Palm, B. B., Romer, P., Stone, E. A., Wooldridge, P. J. and Brown, S. S.: Biomass burning dominates brown carbon absorption in the rural southeastern United States, Geophys. Res. Lett., 42(2), 653–664, doi:10.1002/2014GL062444, 2015.

Weingartner, E., Saathoff, H., Schnaiter, M., Streit, N., Bitnar, B. and Baltensperger, U.: Absorption of light by soot particles: Determination of the absorption coefficient by means of aethalometers, J. Aerosol Sci., 34(10), 1445–1463, doi:10.1016/S0021-8502(03)00359-8, 2003.

Wu, D., Mao, J. T., Deng, X. J., Tie, X. X., Zhang, Y. H., Zeng, L. M., Li, F., Tan, H. B., Bi, X. Y., Huang, X. Y., Chen, J. and Deng, T.: Black carbon aerosols and their radiative properties in the Pearl River Delta region, Sci. China, Ser. D Earth Sci., 52(8), 1152–1163, doi:10.1007/s11430-009-0115-y, 2009.

Wu, D., Wu, C., Liao, B., Chen, H., Wu, M., Li, F., Tan, H., Deng, T., Li, H., Jiang, D. and Yu, J. Z.: Black carbon over the South China Sea and in various continental locations in South China, Atmos. Chem. Phys., 13(24), 12257–12270, doi:10.5194/acp-13-12257-2013, 2013.

Yan, C., Zheng, M., Bosch, C., Andersson, A., Desyaterik, Y., Sullivan, A. P., Collett, J. L., Zhao, B., Wang, S., He, K. and Gustafsson, Ö.: Important fossil source contribution to brown carbon in Beijing during winter, Nat. Publ. Gr., 1–10, doi:10.1038/srep43182, 2017.

Yuan, J. F., Huang, X. F., Cao, L. M., Cui, J., Zhu, Q., Huang, C. N., Lan, Z. J. and He, L. Y.: Light absorption of brown carbon aerosol in the PRD region of China, Atmos. Chem. Phys., 16(3), 1433–1443, doi:10.5194/acp-16-1433-2016, 2016.

Zhu, C.-S., Cao, J.-J., Hu, T.-F., Shen, Z.-X., Tie, X.-X., Huang, H., Wang, Q.-Y., Huang, R.-J., Zhao, Z.-Z., Močnik, G. and Hansen, A. D. A.: Spectral dependence of aerosol light absorption at an urban and a remote site over the Tibetan Plateau, Sci. Total Environ., 590–591(97), 14–21, doi:10.1016/j.scitotenv.2017.03.057, 2017.

Zou, Y., Deng, X. J., Zhu, D., Gong, D. C., Wang, H., Li, F., Tan, H. B., Deng, T., Mai, B. R., Liu, X. T. and Wang, B. G.: Characteristics of 1 year of observational data of VOCs, NO_x and O_3 at a suburban site in Guangzhou, China, Atmos. Chem. Phys., 15(12), 6625–6636, doi:10.5194/acp-15-6625-2015, 2015.

449 Table

450 Table 1. Multilinear regression analyses between b_{BrC} at each wavelength and mass loading of
451 different OA factors from AMS-PMF/ME-2.

	370 nm		470 nm		520 nm		590 nm		660 nm	
	Correlation factor (m^2 g^{-1})	Contribution to b_{BrC}	Correlation factor (m^2 g^{-1})	Contribution to b_{BrC}	Correlation factor (m^2 g^{-1})	Contribution to b_{BrC}	Correlation factor (m^2 g^{-1})	Contribution to b_{BrC}	Correlation factor (m^2 g^{-1})	Contribution to b_{BrC}
HOA	0.61 ± 0.05	22.7%	0.38 ± 0.03	25.4%	0.22 ± 0.02	24.5%	0.16 ± 0.02	25.1%	0.16 ± 0.01	27.9%
BBOA	3.4 ± 0.41	25.2%	1.2 ± 0.26	15.9%	0.63 ± 0.18	13.9%	0.43 ± 0.14	13.4%	0.21 ± 0.11	10.3%
LVOOA	1.04 ± 0.08	52.2%	0.65 ± 0.05	58.7%	0.41 ± 0.04	61.5%	0.29 ± 0.03	61.5%	0.26 ± 0.02	61.3%

452

453 Notes: 1) Correlation coefficient (R) for each regression analysis: 0.65 at 370 nm, 0.58 at 470 nm, 0.51 at 520 nm,
454 0.51 at 570 nm and 0.54 at 660 nm; 2) The correlation factors for COA and SVOOA are near zero at all wavelength,
455 indicating a negligible contribution from these factors. So only the correlation factors for HOA, BBOA and LVOOA
456 are listed in the table

457

458

459 Figures

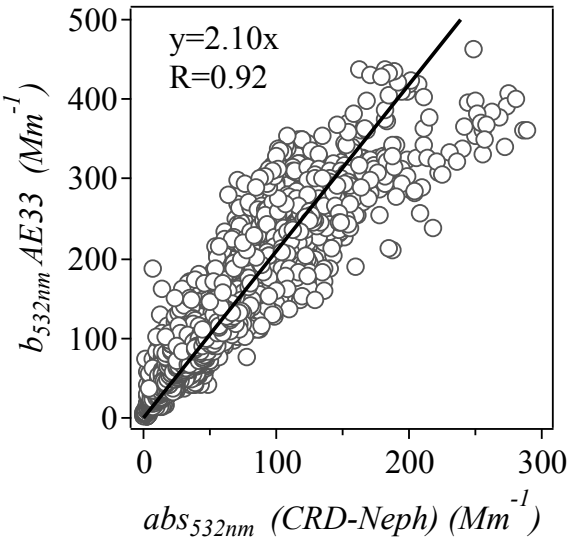

460

461 Figure 1. Scatter plot of absorption coefficients at 532 nm measured with aethalometer (AE33)
462 and those estimated from cavity ring-down spectroscopy (CRD) and Nephelometer measurements.
463

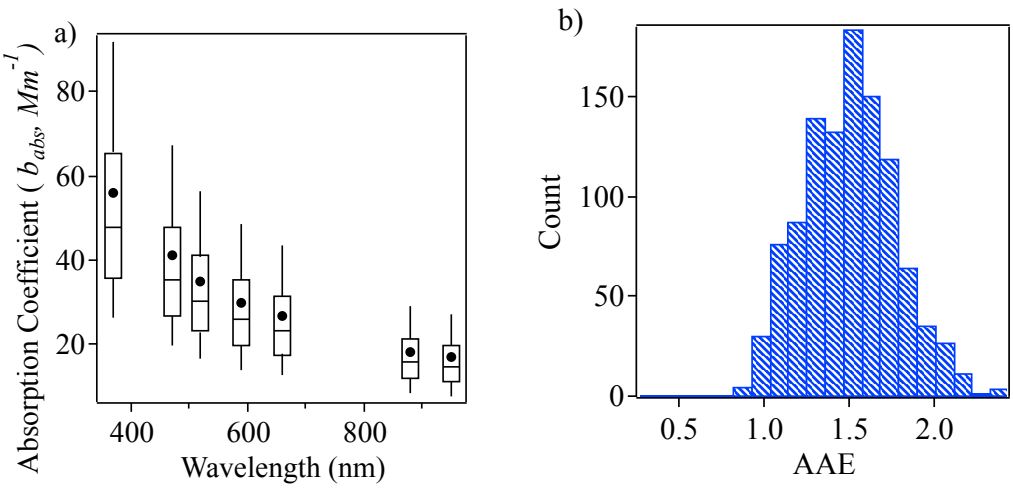

Figure 2. a) Box-whisker plot of absorption coefficient at seven wavelengths as measured with the AE33; b) Histogram of AAE values over the measurement campaign.

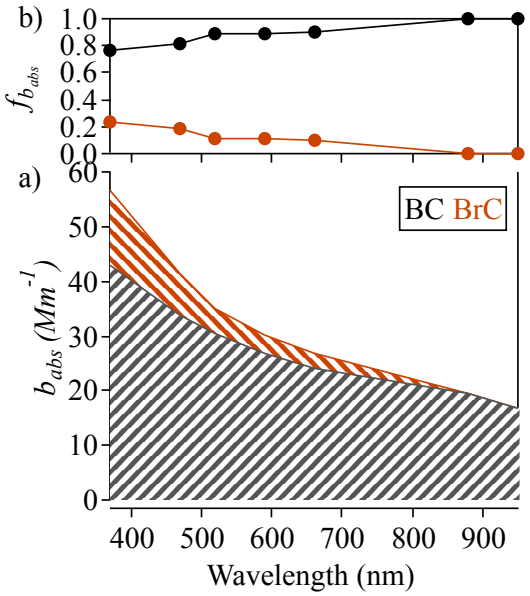

468

469 Figure 3. a) Fractions of BC and BrC contributions to aerosol particle light absorption at different
470 wavelengths; b) Contributions of BC and BrC to the total light absorption coefficient at different
471 wavelengths.

472

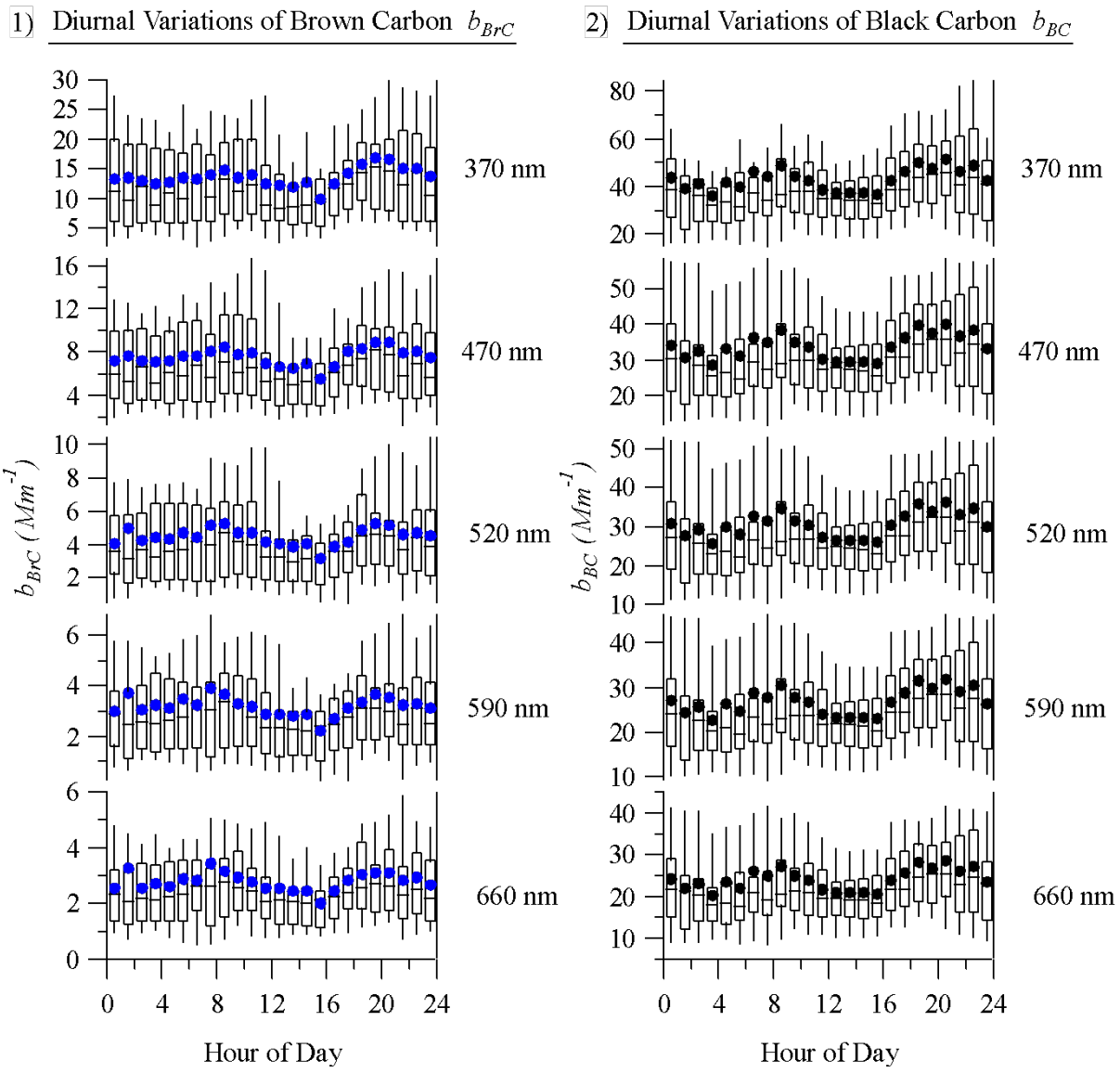

Figure 4. Diurnal variations of BrC and BC light absorption coefficients (b_{BrC} and b_{BC}) at different wavelengths.

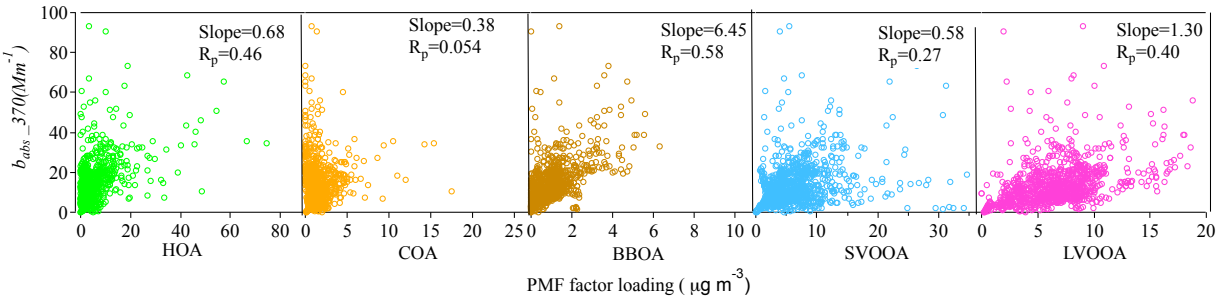

Figure 5. Correlations between the BrC absorption coefficients at 370 nm and the mass loadings of OA factors resolved by AMS-PMF/ME-2.

483

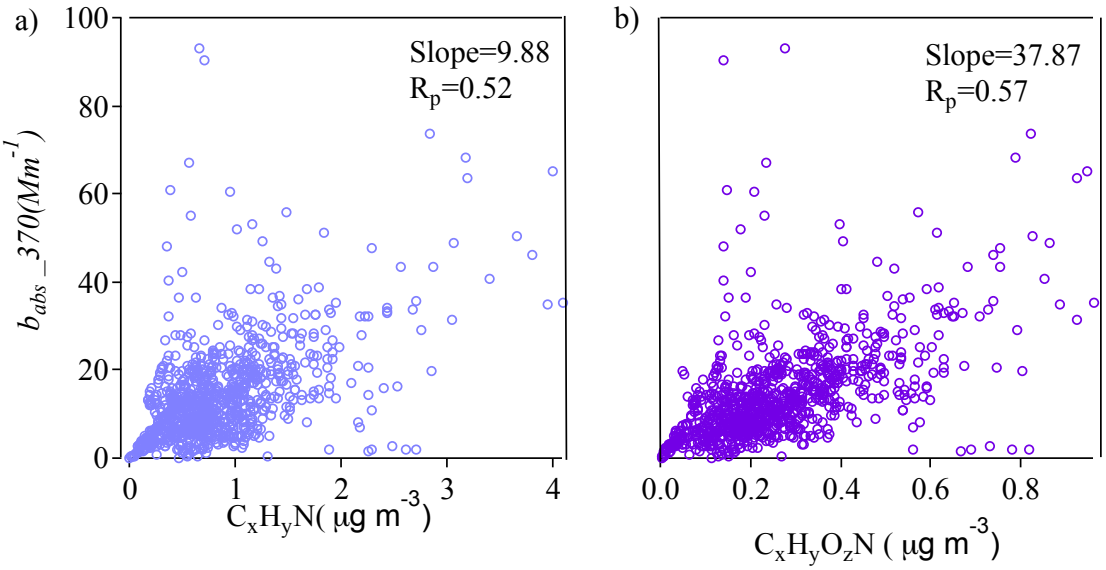

484

485 Figure 6. Correlations between BrC absorption coefficients at 370 nm and mass concentrations of
486 N-containing organic ion families.

487

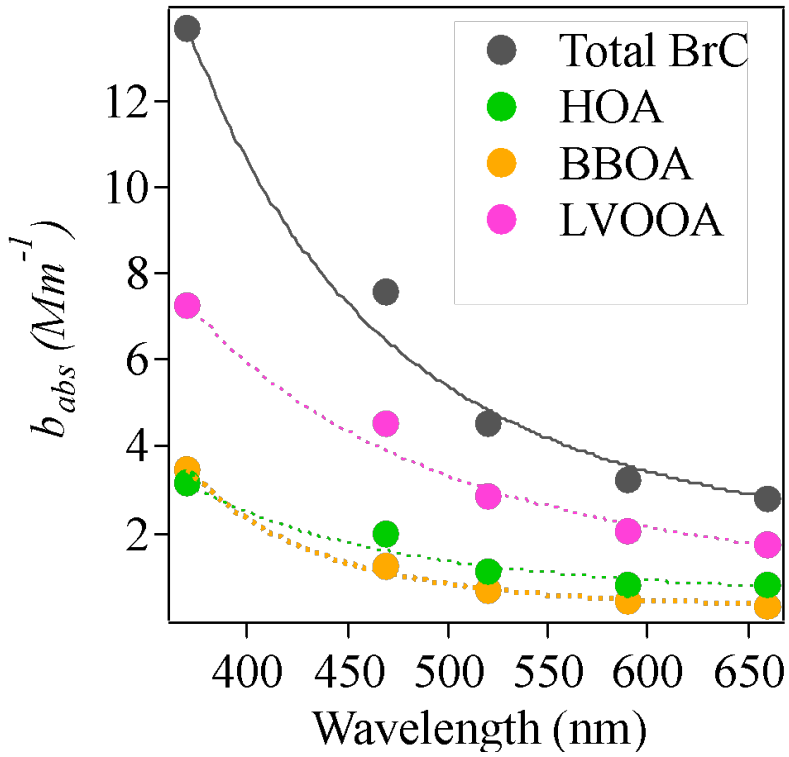

Figure 7. Exponential decay of b_{abs} for total BrC and different light-absorbing OA components across wavelength.

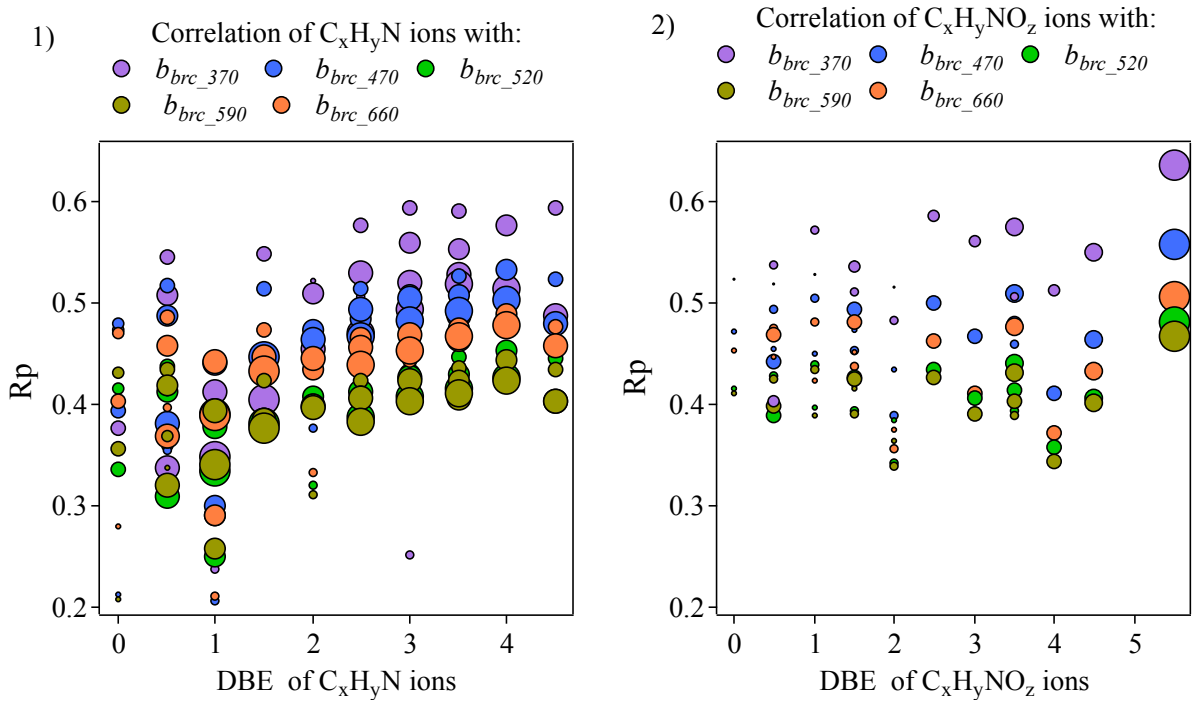

Figure 8. Correlation coefficients between BrC absorption coefficient across different wavelength and N-containing organic ion fragments grouped by double bond equivalence (panels a and b). Larger grey dots correspond to higher carbon numbers.